J. Shanghai Jiaotong Univ. (Sci.), 2016, 21(1): 103-111
DOI: 10.1007/s12204-015-1689-5

Dynamic Response Analysis of a Multi-Column Tension-Leg-Type Floating Wind Turbine Under Combined Wind and Wave Loading

ZHAO Yongsheng (赵永生), *YANG Jianmin* (杨建民), *HE Yanping** (何炎平), *GU Mintong* (顾敏童)
(State Key Laboratory of Ocean Engineering, Shanghai Jiaotong University, Shanghai 200240, China)

Abstract: Floating wind turbines (FWTs) are subjected to combined aerodynamic and hydrodynamic loads varying both in time and amplitude. In this study, a multi-column tension-leg-type FWT (i.e., WindStar TLP system) is investigated for its global performance under normal operating conditions and when parked. The selected variables are analysed using a fully coupled aero-hydro-servo-elastic time domain simulation tool FAST. Three different loading scenarios (wind only, wave only and both combined) are examined to identify the dominant load influencing each response. The key response variables are obtained and compared with those for an NREL 5 MW baseline wind turbine installed on land. The results should aid the detailed design of the WindStar TLP system.
Key words: floating wind turbine (FWT), time domain response, wind and wave loading
CLC number: U 661 **Document code:** A

0 Introduction

Offshore wind energy is the fastest growing renewable energy source and is attracting an increasing attention worldwide. The deep waters around, for example, the United States, Norway, China and Japan have high-quality offshore wind resources[1] that can be economically exploited using floating wind turbines (FWTs). An FWT broadly comprises a floating support platform, upon which the turbine tower and the rotor nacelle assembly (RNA) are mounted, along with the safety and control systems, and the mooring and cable systems[2]. Unlike those on land, offshore turbines are subjected to both wind and waves. Therefore, fully coupled time domain analysis is recommended for such turbines, given its ability to solve the equations of motion for the combined responses of FWTs. Several researchers have studied the dynamic motion responses, mooring loads and instabilities of FWTs[3-5]. Tension-leg-type floating turbines are promising for offshore wind farms, and a multi-column tension-leg-type platform (i.e., WindStar TLP system) designed for an NREL offshore 5 MW baseline wind turbine was proposed in previous work[6]. The support platform has a central column with three radiating corner columns and pontoons. The tendon system consists of a vertical mooring system attached to the end of the tendon support structures (TSSs).

In this work, the coupled dynamic response of the WindStar TLP system is analysed using a fully coupled aero-hydro-servo-elastic time domain simulation tool FAST[7]. Design load cases (DLCs) including normal operation and parked conditions are investigated. Load cases of wind only, wave only and both combined are assessed separately on the WindStar TLP system to find the load driving each excitation. A land-based system comprising the NREL offshore 5 MW baseline wind turbine installed on land[8] is compared with a similar turbine on the WindStar TLP system.

1 Description of the FWT System

1.1 Wind Turbine RNA

The NREL offshore 5 MW baseline wind turbine is a representative utility-scale multi-megawatt turbine. It has three variable-speed blades in an upwind configuration with variable blade-pitch-to-feather control[8]. A conventional control system is implemented with a generator-torque controller for maximising power capture below the rated wind speed and a blade-pitch controller designed to regulate rotor speed above the rated wind speed to minimise the drivetrain load. Figure 1 illustrates the turbine's steady state responses with respect to wind speed (v_{wind}). Table 1 summarises its technical specifications.

Received date: 2014-05-10
Foundation item: the National Basic Research Program (973) of China (No. 2014CB046205)
***E-mail:** hyp110@sjtu.edu.cn

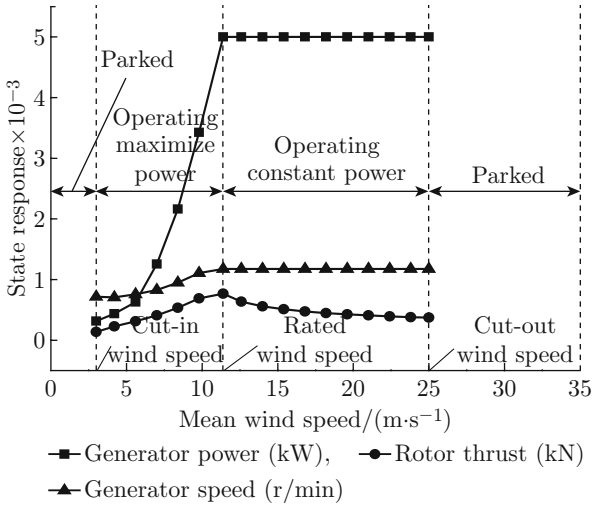

Fig. 1 Steady state results from the NREL 5 MW wind turbine

Table 1 Main properties of the NREL 5 MW baseline wind turbine

Item	Description
Wind turbine class	IEC 61400-3, I_B
Rotor orientation, configuration	Upwind, 3 blades
Rotor, hub diameter	126 m, 3 m
Control strategy	Variable speed, collective pitch
Cut-in, rated, cut-out wind speed	3 m/s, 11.4 m/s, 25 m/s
Cut-in, rated rotor speed	6.9 r/min, 12.1 r/min
Overhang, shaft tilt, precone	5 m, 5°, 2.5°
Rotor, nacelle mass	110 t, 240 t

1.2 Turbine Tower

A turbine tower requires strengthening when mounted on a floating foundation[3]. Therefore, its diameter and thickness are enlarged from the reference structure of the land-based system[8]. The modified tower cross-sectional properties applied in this study are listed in Table 2 (d_{out} is outer diameter; δ is thickness). The overall length of the turbine tower is 65.6 m. Its total structural weight is approximately 266 t, with the centre of mass 26.5 m above the tower base.

Table 2 Turbine tower cross-sectional properties

Elevation/m	d_{out}/m	δ/mm	Point mass/t
0.0	5.600	50	—
6.0	5.454	46	—
12.0	5.307	40	—
24.0	5.015	36	1.5
36.0	4.722	32	—
48.0	4.429	28	—
60.0	4.137	24	—
65.6	4.000	22	1

1.3 The WindStar TLP Support Platform

The WindStar TLP support platform has one central and three equivalent radiating corner columns, pontoons and TSSs. In order to better transfer the large wind overturning moment and minimise the stress concentration at the tower base, the wind turbine tower is designed to install directly on the central column. The corner columns contribute to the external stability during operation, wet-tow transportation, installation and tendon removal. Three TSSs are employed to support the tendons and reduce the dynamic tendon tensions. They also increase the yaw stiffness during operation. At each end of the TSS, a pair of tendons consisting of two polyester ropes are arranged to secure redundancy. The configuration of the proposed WindStar TLP system is shown in Fig. 2 and its main parameters are listed in Table 3. The natural frequencies of the system are obtained by performing linearisation analysis using the FAST model (Table 4).

Table 3 Principal parameters of the WindStar TLP foundation

Parameter	Value
Centre column diameter/m	4.5
Corner column sectional dimension/(m · m)	5.4 × 4.2
Distance between the centre column and corner column/m	20.8
Moulded depth/m	51.3
Design draft/m	30.0
Platform mass (including outfitting) $\times 10^{-3}$/t	1.950
Water ballast/t	500.0
CM location of the platform above keel/m	20.0
Roll inertia about CM $\times 10^{-6}/(t \cdot m^2)$	1.142
Pitch inertia about CM $\times 10^{-6}/(t \cdot m^2)$	1.142
Yaw inertia about CM $\times 10^{-6}/(t \cdot m^2)$	1.373
Number of tendons	6 (3 pairs)
Radius to fairleads/m	40.7
Elastic modulus/MN	391.0
Minimum breaking load/MN	14.72
Pre-tension $\times 10^{-3}$/t	2.400
Total displacement $\times 10^{-3}$/t	5.460

Table 4 Natural frequencies of the WindStar TLP system

Mode	Natural frequency/Hz
Platform surge/sway	0.022 8
Platform heave	0.300
Platform roll, pitch, yaw	0.240, 0.241, 0.038
First tower side-side, fore-aft	1.162, 1.084

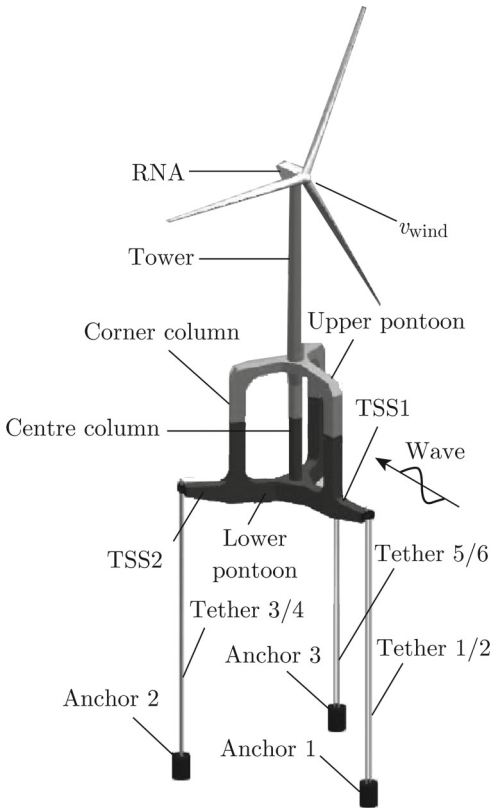

Fig. 2 Configuration of the proposed WindStar TLP system

2 Environmental Conditions and Load Cases

The assumed installation site is located at 61°20′N latitude and 0°0′E longitude, near the Shetland Islands, north-east of mainland Scotland, UK. The water depth at the site is 160 m below mean sea level. The wind and wave conditions are assumed to be described by the 10 min average wind speed v_{aw} at the hub height, the significant wave height H_{s} and the peak spectral period T_{p}. The joint-probability distribution for wind and waves is provided from 37 992 samples, approximately 13 years of data[4]. The IEC 61400-1 design standard[9] is selected here as a guide for the land-based turbine system. The IEC 61400-3 design standard[10] is chosen for the floating system. Two different sets of DLCs, accounting for operating and parked conditions, are considered here (Table 5). DLC01 to DLC15 consider power production under normal operation with the control system fully enabled over a range of wind speeds and wave conditions. DLC16 and DLC17 consider parked (idling) conditions with the control system shut down under extreme load cases with 1- and 50-year return periods; the associated extreme wind speeds, denoted as $v_{1\text{-year}}$ and $v_{50\text{-year}}$ respectively, are 38 and 47.5 m/s. The winds and waves are considered collinear.

Table 5 Summary of selected design load cases

DLCs	$v_{\text{aw}}/(\text{m}\cdot\text{s}^{-1})$	H_{s}/m	T_{p}/s	Turbine status
01	4.2	1.7	12.7	Operating
02	5.6	1.8	12.7	Operating
03	7.0	1.9	12.7	Operating
04	8.4	2.0	14.8	Operating
05	9.8	2.2	13.4	Operating
06	11.2	2.4	13.4	Operating
07	12.6	2.7	12.7	Operating
08	14.0	3.0	12.0	Operating
09	15.4	3.4	13.4	Operating
10	16.8	3.7	13.4	Operating
11	18.2	4.1	15.5	Operating
12	19.6	4.4	14.1	Operating
13	21.0	4.7	13.4	Operating
14	22.4	5.2	16.2	Operating
15	23.8	5.5	15.5	Operating
16	38.0	11.8	17.6	Parked
17	47.5	15.0	19.2	Parked

3 Time Domain Coupled Dynamic Analysis

3.1 Definition of Support Platform Rigid-body Motion Modes

The WindStar TLP support platform is considered as a rigid body with six degrees of freedom (DoFs): three translational (surge, sway, heave) and three rotational (roll, pitch, yaw), as shown in Fig. 3. The right-handed coordinate system has positive z running vertically upward through the centre of gravity of the body,

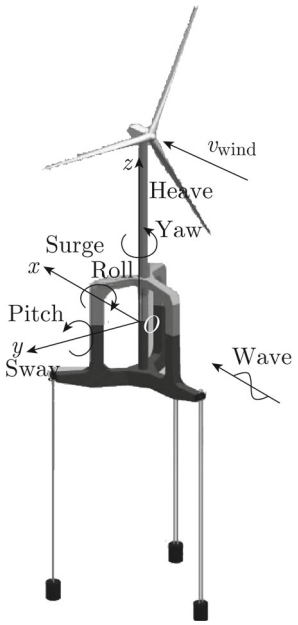

Fig. 3 The coordinate system and support platform degrees of freedom

with the origin in the plane of the mean sea level. The translational displacements in the x, y and z directions with respect to the origin (respectively surge, sway and heave) are labelled η_1, η_2 and η_3, respectively. The angular displacements in the rotational motion of the roll, pitch and yaw about the x, y and z axes are labelled η_4, η_5 and η_6, respectively.

3.2 Equations of Motion

The complete nonlinear time-domain equations of motion of the coupled turbine RNA, tower, support platform and mooring system are of the general form[4]:

$$M_{ij}(\eta, u, t)\ddot{\boldsymbol{\eta}}_j = \boldsymbol{F}_i(\eta, \dot{\eta}, u, t), \tag{1}$$

where, M_{ij} is the (i, j) component of the inertia mass matrix, depending on a nonlinear combination of system displacement η, control input u and time t; $\ddot{\boldsymbol{\eta}}_j$ is the system acceleration of DoF j; $\boldsymbol{F}_i$ is the force component associated with DoF i, depending on a nonlinear combination of system displacement η, system velocity $\dot{\eta}$, control input u and time t. FAST[7] is applied to solving the above equations of motion.

3.3 Aerodynamic Loads

Blade element momentum (BEM) theory, based on blade element theory and blade momentum theory, is one of the most commonly used methods for calculating aerodynamic loads on wind turbine blades. Blade element theory calculates the aerodynamic forces at a section of the blade based on the blade geometry and the local flow conditions. These elemental forces are summed along the span of the blade to calculate the total forces and moments exerted on the turbine. Blade momentum theory assumes that the loss of pressure or momentum in the rotor plane is caused by the work done by the airflow passing through the rotor plane on the blade elements. Based on the momentum theory, the induced velocities from the momentum lost in the flow in the axial and tangential directions can be determined. BEM can provide very satisfactory results, provided that it is supplied with good aerofoil data (for the lift and drag coefficients with respect to the angle of attack) and, if possible, the Reynolds number[11-13].

The relative speed v_{rel} of the blade element moving within the airflow can be expressed as

$$v_{\mathrm{rel}} = v\sqrt{(1-a)^2 + \left[\frac{r\Omega_r}{v}(1+a')\right]^2}, \tag{2}$$

$$\alpha = \phi - \beta, \tag{3}$$

$$\tan\phi = \frac{v}{\Omega_r r}\frac{1-a}{1+a'}, \tag{4}$$

where, a and a' are the axial and angular induction factors, respectively; r is the distance of the aerofoil section from the blade root; v is the upstream wind velocity; α is the angle of attack; ϕ is the relative angle of the wind; β is the section pitch angle; Ω_r is the angular velocity. Figure 4 shows a transverse-sectional view of the blade structure.

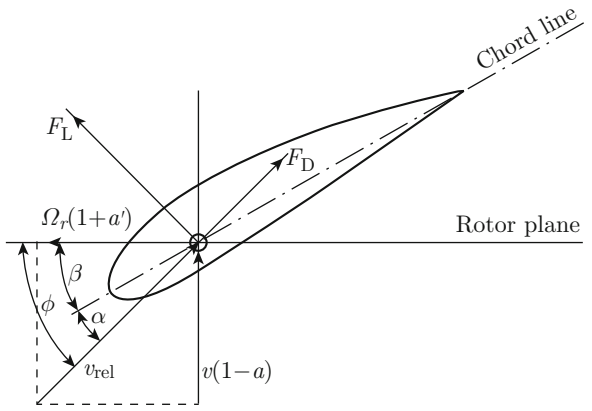

Fig. 4 Local elemental aerodynamic forces

In order to obtain maximum power, a and a' must be related as follows[12]:

$$a' = \frac{1-3a}{4a-1}. \tag{5}$$

The lift F_{L} and drag F_{D} forces for each blade element are generally expressed in terms of the lift and drag coefficients C_{L} and C_{D} as follows:

$$F_{\mathrm{L}} = \frac{\rho_{\mathrm{air}} c}{2} v_{\mathrm{rel}}^2 C_L(\alpha)\Delta r, \tag{6}$$

$$F_{\mathrm{D}} = \frac{\rho_{\mathrm{air}} c}{2} v_{\mathrm{rel}}^2 C_D(\alpha)\Delta r, \tag{7}$$

where c is the aerofoil chord length, Δr is the radial length of the blade sections, and ρ_{air} is the density of air.

The axial force F_{T} on the rotor is a combination of the lift and drag forces, as given by

$$F_{\mathrm{T}} = F_{\mathrm{L}}\cos\phi + F_{\mathrm{D}}\sin\phi. \tag{8}$$

The AeroDyn (v13.0)[13] aerodynamic module of FAST[7] is used to calculate the aerodynamic forces and moments on the rotor. Both BEM and the generalized dynamic wake options, including the effects of axial and tangential induction, are provided. Tip losses, hub losses and the Beddoes-Leishman dynamic stall corrections[11] are implemented in all the simulations.

3.4 Hydrodynamic Loads

Hydrodynamic loads result from the integration of the dynamic pressure of the water over the wetted surface of the support platform and include contributions from inertia (added mass), linear drag (radiation), buoyancy (restoring), incident wave scattering (diffraction), current and nonlinear effects[14].

The hydrodynamic load $\boldsymbol{F}_i^{\mathrm{Hyd}}$ acting on the six DoFs of the support platform can be split into three parts: a

linear potential wave load $\boldsymbol{F}_i^{\text{Wave}}$, a nonlinear viscous-drag load $\boldsymbol{F}_i^{\text{Vis}}$ and a hydrostatic load $\boldsymbol{F}_i^{\text{Hys}}$. The total hydrodynamic load is the sum of these loads:

$$\boldsymbol{F}_i^{\text{Hyd}} = \boldsymbol{F}_i^{\text{Wave}} + \boldsymbol{F}_i^{\text{Vis}} + \boldsymbol{F}_i^{\text{Hys}}. \tag{9}$$

The linear potential wave forces can be split into two terms:

$$\boldsymbol{F}_i^{\text{Wave}} = \boldsymbol{F}_i^{\text{Rad}} + \boldsymbol{F}_i^{\text{Diff}}. \tag{10}$$

The radiation force is related to the hydrodynamic loads on the floater due to forced oscillations of the floater in all its DoFs when no incident surface waves are present. The resulting radiation loads include contributions from added mass and force which are proportional to the floater accelerations, and contributions from radiation damping which are proportional to the floater velocity.

$$\boldsymbol{F}_i^{\text{Rad}} = -\boldsymbol{A}_{ij}(\omega)\ddot{\boldsymbol{\eta}}_j(t) - \boldsymbol{B}_{ij}(\omega)\dot{\boldsymbol{\eta}}_j(t), \tag{11}$$

where $\boldsymbol{A}_{ij}(\omega)$ is the added mass coefficient matrix, and $\boldsymbol{B}_{ij}(\omega)$ is the damping coefficient matrix.

The radiation force can be determined in the time domain by taking the inverse transform of the radiation loads in the frequency domain:

$$\boldsymbol{F}_i^{\text{Rad}} = -\boldsymbol{A}_{ij}(\infty)\ddot{\boldsymbol{\eta}}_j(t) - \int_0^t \boldsymbol{h}_{ij}(t-\tau)\dot{\boldsymbol{\eta}}_j(\tau)\mathrm{d}\tau, \tag{12}$$

where τ is the dummy variable with the same unit as the simulation time, $\boldsymbol{A}_{ij}(\infty)$ is the added mass coefficient at infinite frequency, and $\boldsymbol{h}_{ij}(\tau)$ is the retardation function expressed by

$$\boldsymbol{h}_{ij}(\tau) = \frac{2}{\pi}\int_0^\infty \boldsymbol{B}_{ij}(\omega)\cos(\omega\tau)\mathrm{d}\omega. \tag{13}$$

The diffraction force can be defined as the total excitation load acting on the support platform from incident waves. Considering stochastic sea states defined by an appropriate wave spectrum, the wave elevation $\varsigma(t)$ and diffraction loads $\boldsymbol{F}_i^{\text{Diff}}$ are given by[14]

$$\varsigma(t) = \frac{1}{2\pi}\int_{-\infty}^{\infty} W(\omega)\sqrt{2\pi S_\eta^{\text{2-sided}}(\omega)}\mathrm{e}^{\mathrm{j}wt}\mathrm{d}\omega, \tag{14}$$

$$\boldsymbol{F}_i^{\text{Diff}} = \frac{1}{2\pi}\int_{-\infty}^{\infty} W(\omega)\sqrt{2\pi S_\eta^{\text{2-sided}}(\omega)}\times \boldsymbol{X}_i(\omega,\beta)\mathrm{e}^{\mathrm{j}wt}\mathrm{d}\omega, \tag{15}$$

where $S_\eta^{\text{2-sided}}(\omega)$ is the power spectral density of the two-sided wave spectrum, $W(\omega)$ represents the Fourier transform of realisation of a white Gaussian noise time-series process with zero mean and unit variance, and $\boldsymbol{X}_i(\omega,\beta)$ is the wave excitation force on the support platform, normalised per unit wave amplitude.

The viscous-drag load is defined by the Morison equation and expressed by

$$\boldsymbol{F}_i^{\text{Vis}} = \frac{1}{2}\boldsymbol{C}_{\text{d}}\rho_{\text{w}}A[\boldsymbol{\eta}_i(t) - \boldsymbol{\varsigma}_i(t)]|\boldsymbol{\eta}_i(t) - \boldsymbol{\varsigma}_i(t)|, \tag{16}$$

where $\boldsymbol{\varsigma}_i(t)$ is the undisturbed flow velocity taken at the instantaneous position of the centre of gravity, $\boldsymbol{C}_{\text{d}}$ is the viscous coefficient in the specific direction that has projection area A, and ρ_{w} is the density of seawater.

The hydrostatic loads $\boldsymbol{F}_i^{\text{Hys}}$ include the buoyancy force from the Archimedes' principle and the linear hydrostatic restoring force from the effects of the water-plane area A_{wp} and the centre of buoyancy (CoB):

$$\boldsymbol{F}_i^{\text{Hys}} = \rho_{\text{w}}gV_0\boldsymbol{v}_{i,3} - \boldsymbol{C}_{ij}^{\text{Hys}}\boldsymbol{\eta}_j(t), \tag{17}$$

where, V_0 is the volume of water displaced when the support platform is in its undisplaced position; g is the gravitational constant; $\boldsymbol{v}_{i,3}$ is the $(i,3)$ component of the Kronecker-Delta function, nonzero only when DoF $i=3$. For the support platform with the x-z plane as a plane of symmetry for the wetted hull, the assumption of small angles leads to the linearised hydrostatic restoring coefficient matrix $\boldsymbol{C}_{ij}^{\text{Hys}}$ having the following form (z_{CoB} is the vertical position of the CoB):

$$\boldsymbol{C}_{ij}^{\text{Hys}} = \begin{bmatrix} 0 & 0 & 0 & 0 & 0 & 0 \\ 0 & 0 & 0 & 0 & 0 & 0 \\ 0 & 0 & \rho_{\text{w}}gA_{\text{wp}} & 0 & -\rho_{\text{w}}g\iint_{A_{\text{wp}}} x\mathrm{d}A & 0 \\ 0 & 0 & 0 & \rho_{\text{w}}g\iint_{A_{\text{wp}}} y^2\mathrm{d}A + \rho_{\text{w}}gV_0z_{\text{COB}} & 0 & 0 \\ 0 & 0 & -\rho_{\text{w}}g\iint_{A_{\text{wp}}} x\mathrm{d}A & 0 & \rho_{\text{w}}g\iint_{A_{\text{wp}}} x^2\mathrm{d}A + \rho_{\text{w}}gV_0z_{\text{COB}} & 0 \\ 0 & 0 & 0 & 0 & 0 & 0 \end{bmatrix}. \tag{18}$$

The HydroDyn (v2.0) hydrodynamic module of FAST[7] is used to simulate irregular waves and calculate hydrodynamic loads on the support platform. The linearised radiation and diffraction loads are obtained using the code Wadam[15], a frequency-domain hydrodynamic analysis program based on the three-dimensional numerical panel method, to calculate wave-structure interaction for fixed and floating structures.

3.5 Mooring Loads

Mooring loads from the tension mooring system can be defined by assuming linearity and by ignoring the inertia and damping of the mooring line:

$$\boldsymbol{F}_i^{\text{Mooring}} = \boldsymbol{F}_i^{\text{Pre}} - \boldsymbol{C}_{ij}^{\text{Mooring}}\boldsymbol{\eta}_j(t), \tag{19}$$

where $\boldsymbol{F}_i^{\text{Pre}}$ is the ith component of the total pre-tension load of the tension mooing system, and $\boldsymbol{C}_{ij}^{\text{Mooring}}$ is the linearised restoring stiffness matrix of the mooring system due to the elastic properties of the tendons and the weight of the tendons in the water. The coupled restoring stiffness matrix can be determined by[16]

$$\boldsymbol{C}_{ij}^{\text{Mooring}} = \begin{bmatrix} C_{11} & 0 & 0 & 0 & 0 & 0 \\ 0 & C_{22} & 0 & 0 & 0 & 0 \\ C_{31} & C_{32} & C_{33} & C_{34} & C_{35} & C_{36} \\ 0 & C_{42} & 0 & C_{44} & 0 & 0 \\ C_{51} & 0 & 0 & 0 & C_{55} & 0 \\ 0 & 0 & 0 & 0 & 0 & C_{66} \end{bmatrix} \begin{matrix} \text{Surge} \\ \text{Sway} \\ \text{Heave} \\ \text{Roll} \\ \text{Pitch} \\ \text{Yaw} \end{matrix}. \tag{20}$$

The mooring loads are calculated using the mooring analysis program[7], which is a multi-segmented, quasi-static mooring solver. They account for the mooring line's apparent weight in fluid, its elastic stretching and the nonlinear geometric restoration of the entire mooring system. The bending stiffness and inertia of individual mooring line are neglected and so does the damping.

4 Results and Discussion

Numerical simulations are carried out in the time domain using the fully coupled aero-hydro-servo-elastic simulation tool FAST. During normal operating conditions (DLC01 to DLC15), 15 simulations of 10 min each are performed for each DLC. Six simulations for 1 h each are conducted under parked conditions (DLC16 and DLC17). Turbulent wind inflow is simulated using the program Turbsim[17]. The Pierson-Moskowitz spectrum is applied to simulating the irregular wave elevation process. Figures 5 and 6 illustrate the time histories of the wind and wave condition applied in DLC07, respectively.

Three different loading scenarios (wind only, wave only and both combined) are examined to identify the driving load of the responses. Global response variables including generator power, blade pitch angle, blade deflection, nacelle acceleration, support platform motion and tendon tension are studied for the specified DLCs. Time series data and associated statistics, including the minimum, maximum, mean and standard deviation, are obtained by 80 Hz sampling. The results are also compared with those for the land-based system.

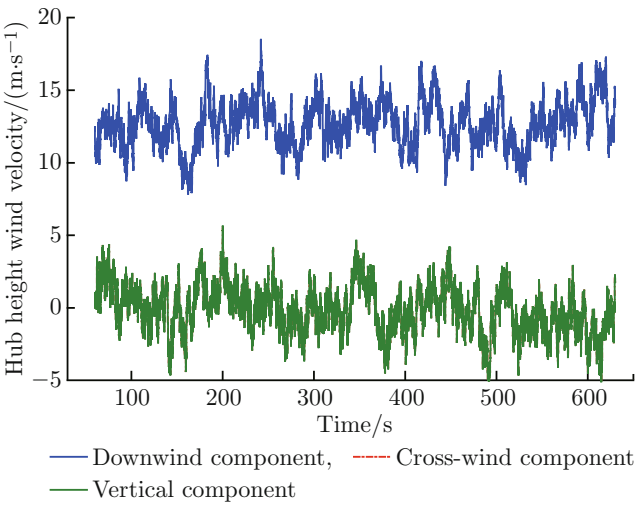

Fig. 5 Time history of hub height wind speed for DLC07

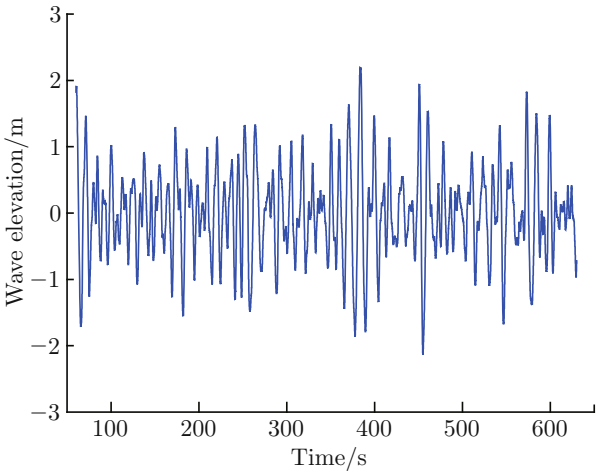

Fig. 6 Time history of wave elevation for DLC07

4.1 Generator Power

Figures 7 and 8 present the time series of generator power and Blade 1 pitch angle for both the land-based system and the WindStar TLP system for DLC07. Both systems achieve a similar generator power output. This is largely attributed to the tension mooring system: the proposed WindStar TLP system has small dynamic motion responses and thus has little effect on the power output. However, the standard deviation of generator power for the WindStar TLP system is increased during turbine operation (Fig. 9), mainly owing to the

motion of the platform under the excitation of the combined wind and wave loads. The incoming wind turbulence at the RNA is greater for the WindStar TLP system than for the land-based system due to the support platform surge velocity and pitch-induced surge velocity.

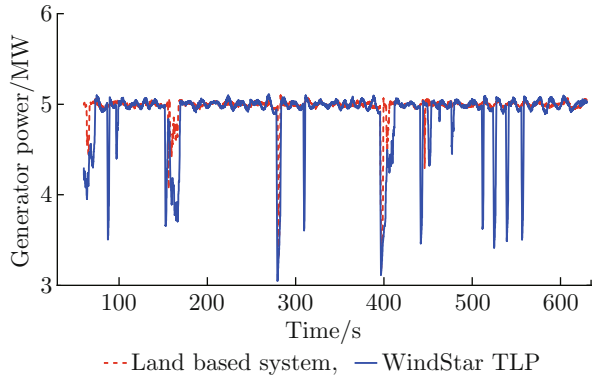

Fig. 7 Time history of generator power for DLC07

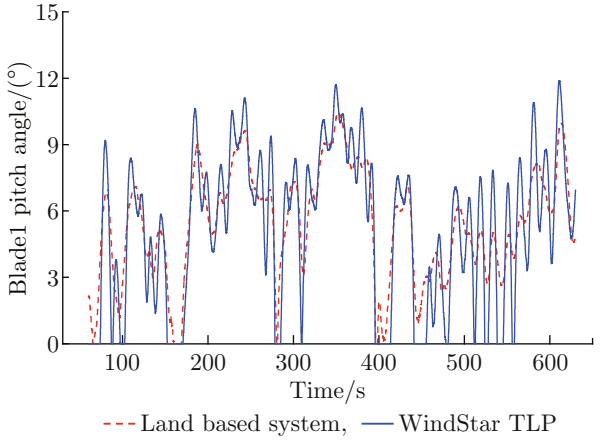

Fig. 8 Time history of blade pitch response for DLC07

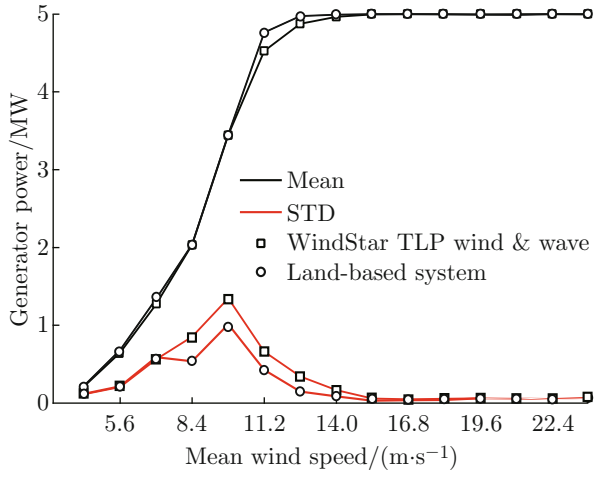

Fig. 9 Statistics of generator power

4.2 Out-of-Plane Blade Deflection

The out-of-plane deflection of Blade 1 during turbine operation (DLC01 to DLC15) is shown in Fig. 10. Clearly, the mean response is mainly induced by wind loads; it shows peak response at the rated wind speed due to the peak rotor thrust. In contrast, the standard deviation of the out-of-plane blade deflection is mainly induced by a combination of support platform motions and wave loads. The maximum responses for both systems occur at DLC08 (v_{aw} = 14.0 m/s), with the maximum deflection for the WindStar TLP system being 12.8% greater than that of the land-based system.

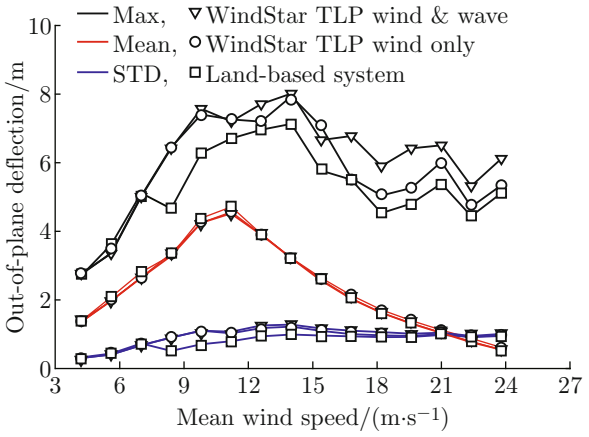

Fig. 10 Out-of-plane deflection of Blade 1

4.3 Nacelle Acceleration

Figure 11 shows the modelled nacelle surge acceleration for both systems, where $v_{cut\text{-}in}$, v_{rated} and $v_{cut\text{-}out}$ are cut-in, rated and cut-out wind speeds, respectively, and a_{ns} is the nacelle surge acceleration. It appears overall higher for the WindStar TLP system than for the land-based system both during operation and when

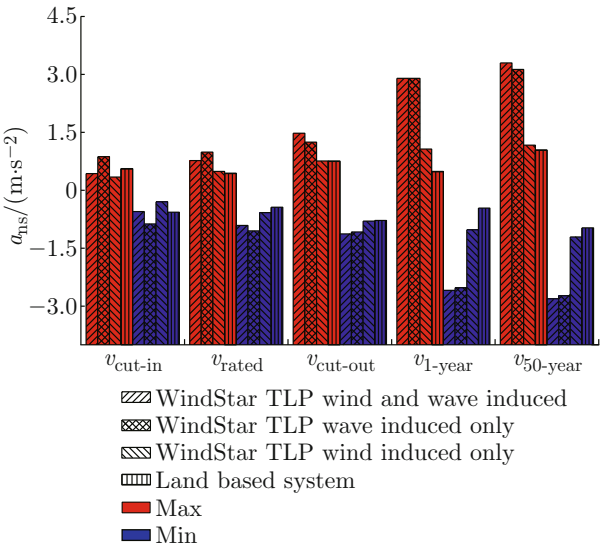

Fig. 11 Statistics of the nacelle surge acceleration

parked. For mean wind speed below the rated speed, the control strategy is to maximize generator power; therefore, there is a positive aerodynamic damping acting on the WindStar TLP system, and the maximum response of nacelle surge acceleration below the rated wind speed under combined wind and wave loading is lower than that in the wave-only case. At mean wind speed higher than the rated speed, the control strategy is to maintain constant power by feathering the blade, thus introducing negative aerodynamic damping. The WindStar TLP system with the turbine parked clearly shows the maximum response of nacelle surge acceleration, mainly induced by waves. The maximum response is about 310% that of the land-based system.

4.4 Platform Motion

Figures 12 and 13 present the maximum surge and pitch motions of the WindStar TLP system with the turbine operating and parked. The results show that the surge and pitch motions near the rated wind speed are mainly induced by wind loads. With the turbine parked, these motions are dominated by the wave loads. The maximum surge and pitch displacement are 13.68 m and 1.31°, respectively, which occur in DLC17 (50-year extreme load case).

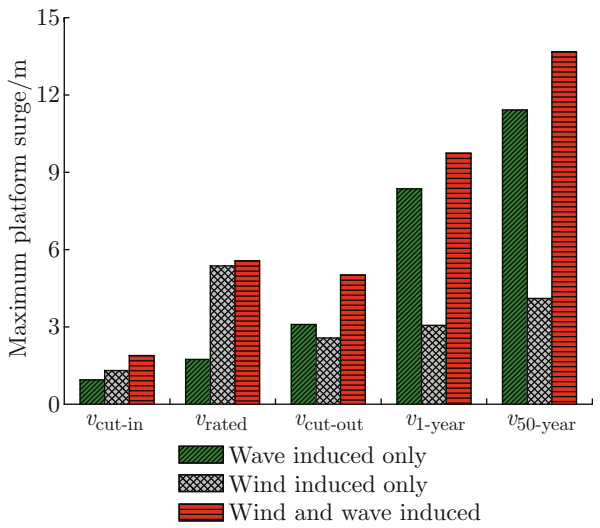

Fig. 12 Maximum response of platform surge

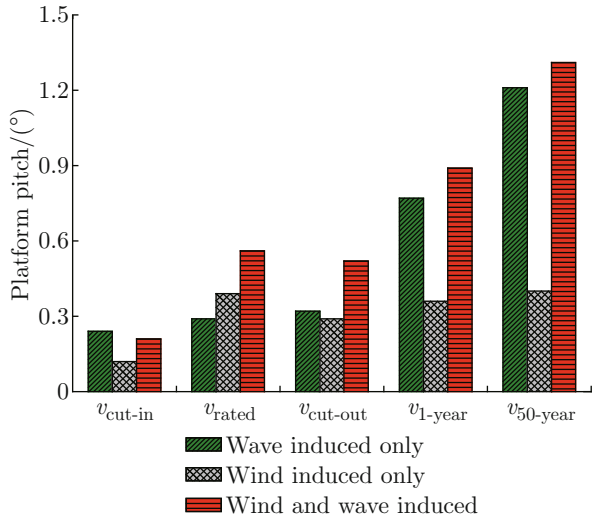

Fig. 13 Maximum response of platform pitch

4.5 Tendon Tension

Figure 14 shows the maximum and minimum upwind tendon tensions (Tendon 1) of the WindStar TLP system with the turbine operating and parked. Tendon tension is highly correlated to platform surge and pitch displacement; consequently, it shows the same trends. Its maximum value (for Tendon 1) is approximately 7.170 MN, including the initial pre-tension. This value gives a safety factor of 2.05. The minimum upwind tendon tension remains positive under all the considered conditions.

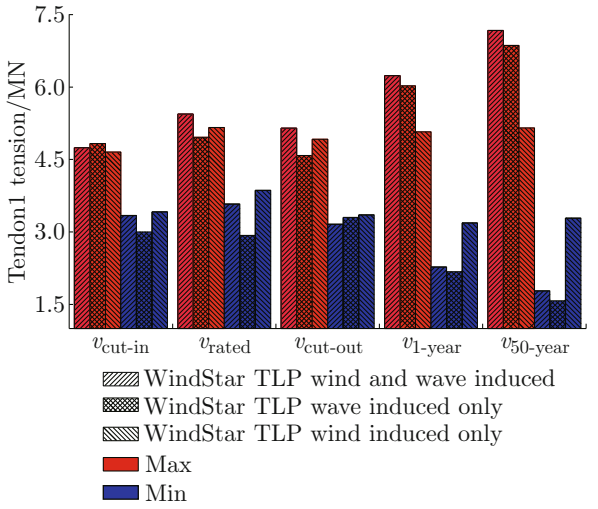

Fig. 14 Statistics of platform upwind tendon tension

5 Conclusion

This work investigates the dynamic responses of the WindStar TLP system under normal operating and parked conditions. The system is quantitatively compared with a land-based system employing a similar turbine. The dominant excitation loads of selected global response variables are identified by the separate modelling of various DLCs: wind only, wave only and both combined.

The proposed WindStar TLP system shows larger out-of-plane blade deflection and nacelle surge acceleration than the land-based system, with ratio up to 1.13 and 3.1, respectively, found during the DLCs considered. The upwind tendon (Tendon 1) has a safety factor of 2.05, and the minimum upwind tendon tension remains positive under all the selected DLCs. These results show the loading difference between the WindStar

TLP system and the land-based system, and therefore aid relevant modifications to the initial design. Future work will focus on performing a comprehensive load analysis according to IEC 61400-3 requirements and testing a scale model in a wave tank.

References

[1] BTM Consult APS. International wind energy development world market update 2009, forecast 2010—2014 [R]. Denmark: BTM Consult APS, 2010.

[2] American Bureau of Shipping. Guidance notes on global performance analysis for floating offshore wind turbine [R]. Houston, USA: American Bureau of Shipping, 2013.

[3] JONKMAN J M. Dynamics of offshore floating wind turbines-model development and verification [J]. *Wind Energy*, 2009, **12**: 459-492.

[4] JONKMAN J M, MATHA D. Dynamics of offshore floating wind turbines-analysis of three concepts [J]. *Wind Energy*, 2011, **14**: 557-569.

[5] KARIMIRAD M, MOAN T. Wave- and wind-induced dynamic response of a spar-type offshore wind turbine [J]. *Journal of Waterway, Port, Coastal, and Ocean Engineering*, 2012, **138**: 9-20.

[6] ZHAO Y S, YANG J M, HE Y P. Preliminary design of a multi-column TLP foundation for a 5-MW offshore wind turbine [J]. *Energies*, 2012, **5**: 3874-3891.

[7] JONKMAN J M, BUHL JR M L. FAST user's guide [R]. Colorado, USA: National Renewable Energy Laboratory, 2005.

[8] JONKMAN J M, BUTTERFIELD S, MUSIAL W, et al. Definition of a 5-MW reference wind turbine for offshore system development [R]. Colorado, USA: National Renewable Energy Laboratory, 2009.

[9] International Electrotechnical Committee. Wind turbine generator systems. Part 1. Design requirements [R]. Geneva, Switzerland: International Electrotechnical Commission, 2005.

[10] International Electrotechnical Commission. Wind turbines. Part 3. Design requirements for offshore wind turbines [R]. Geneva, Switzerland: International Electrotechnical Commission, 2009.

[11] MANWELL J F, MCGOWAN J G, ROGERS A L. Wind energy explained: Theory, design and application [M]. West Sussex, UK: John Wiley & Sons Ltd, 2012.

[12] BURTON T, SHARPE D, JENKINS N, et al. Wind energy handbook [M]. New York, USA: John Wiley & Sons Ltd, 2011.

[13] MORIARTY P J, HANSEN A C. AeroDyn theory manual [R]. Colorado, USA: National Renewable Energy Laboratory, 2005.

[14] JONKMAN J M. Dynamics modeling and loads analysis of an offshore floating wind turbine [R]. Colorado, USA: National Renewable Energy Laboratory, 2007.

[15] Det Norske Veritas. Wadam theory manual [R]. Høvik, Norway: Det Norske Veritas, 2008.

[16] AHMAD S, ISLAM N, ALI A. Wind-induced response of a tension leg platform [J]. *Journal of Wind Engineering and Industrial Aerodynamics*, 1997, **72**: 225-240.

[17] JONKMAN B J, BUHL JR M L. TurbSim user's guide [R]. Colorado, USA: National Renewable Energy Laboratory, 2007.